Seasonal cycling of zinc and cobalt in the Southeast Atlantic along the GEOTRACES GA10 section.

Neil J. Wyatt[1], Angela Milne[2], Eric P. Achterberg[3], Thomas J. Browning[3], Heather A. Bouman[4], E. Malcolm S. Woodward[5], Maeve C. Lohan[1].

[1]Ocean and Earth Science, National Oceanography Centre, University of Southampton, Southampton, United Kingdom.

[2]School of Geography, Earth and Environmental Sciences, University of Plymouth, Plymouth, United Kingdom.

[3]Marine Biogeochemistry Division, GEOMAR Helmholtz Centre for Ocean Research, Kiel, Germany.

[4]Department of Earth Sciences, University of Oxford, Oxford, United Kingdom.

[5]Plymouth Marine Laboratory, Plymouth, United Kingdom.

Correspondence to: N. J. Wyatt (n.j.wyatt@soton.ac.uk)

Abstract

We report the distributions and stoichiometry of dissolved zinc (dZn) and cobalt (dCo) in sub-tropical and sub-Antarctic waters of the Southeast Atlantic Ocean during austral spring 2010 and summer 2011/12. In sub-tropical surface waters, mixed-layer dZn and dCo concentrations during early spring were 1.60 ± 2.58 nM and 30 ± 11 pM, respectively, compared with summer values of 0.14 ± 0.08 nM and 24 ± 6 pM. The elevated spring dZn concentrations resulted from an apparent offshore transport of elevated dZn at depths between $20 - 55$ m, derived from from the Agulhas Bank. In contrast, open-ocean sub-Antarctic surface waters displayed largely

consistent inter-seasonal mixed-layer dZn and dCo concentrations of 0.10 ± 0.07 nM and 11 ± 5 pM, respectively. Trace metal stoichiometry, calculated from concentration inventories, suggest a greater overall removal for dZn relative to dCo in the upper water column of the Southeast Atlantic with an inter-seasonally decreasing dZn/dCo inventory ratios of 19 to 5 mol mol^{-1} and 13 to 7 mol mol^{-1} for sub-tropical surface water and sub-Antarctic surface water, respectively. In this paper, we investigate how the seasonal influences of external input and phytoplankton succession may relate to the distribution of dZn and dCo, and variation in dZn/dCo stoichiometry, across these two distinct ecological regimes in the Southeast Atlantic.

1.   Introduction

The trace metal micronutrients zinc (Zn) and cobalt (Co) play an important role in the productivity of the oceans as key requirements in marine phytoplankton metabolism (Morel, 2008; Twining and Baines, 2013). Zinc is required for the acquisition of inorganic carbon and organic phosphorus via the carbonic anhydrase and alkaline phosphatase metalloenzymes, respectively (Morel et al., 1994; Shaked et al., 2006; Cox and Saito, 2013). The requirement for Co stems from its obligation in the biosynthesis of vitamin B$_{12}$ (Raux et al., 2000; Rodionov et al., 2003) and, like Zn, its potential roles as a metal cofactor in carbonic anhydrase and alkaline phosphatase (Morel et al., 1994; Jakuba et al., 2008; Saito et al., 2017). Significantly, both dissolved Zn (dZn) and Co (dCo) are often scarce in surface seawater with mean concentrations that are often similar to, or relatively depleted, compared with typical cellular requirements of phytoplankton (Moore et al., 2013; Moore, 2016). Hence, dZn and dCo availability have the potential to regulate phytoplankton metabolism and growth rates in some ocean regions (Sunda and Huntsman, 1992; Saito et al., 2002; Franck et al., 2003; Shaked et al., 2006; Bertrand et al., 2007; Jakuba et al., 2012; Mahaffey et al., 2014; Chappell et al., 2016; Browning et al., 2017).

51 The role for Zn and Co in carbonic anhydrase establishes an interaction between their ocean

52 cycles, whereby biochemical substitutions between the enzyme-bound metals enables a

53 stoichiometric plasticity in their cellular requirements that can negate the effect of limited

54 availability. For example, a number of eukaryotic algae can substitute Zn for Co, as well as

55 cadmium (Cd), in carbonic anhydrase when seawater dZn concentrations are low (Price and

56 Morel, 1990; Sunda and Huntsman, 1995; Lane and Morel, 2000; Xu et al., 2007; Saito and

57 Goepfert, 2008; Kellogg et al., 2020). In contrast, the prokaryotic picocyanobacteria

58 *Synechococcus* and *Prochlorococcus* appear to have an absolute Co requirement (Sunda and

59 Huntsman, 1995; Saito et al., 2002; Hawco and Saito, 2018). The availability and stoichiometry

60 of dZn and dCo may therefore also exert a key control on phytoplankton community structure

61 in some ocean regions (Leblanc et al., 2005; Saito et al., 2010; Chappell et al., 2016).

62 With the arrival of GEOTRACES research cruises, a number of studies have provided

63 comprehensive data on the basin-scale distributions of Zn and Co in the Atlantic Ocean (e.g.

64 Bown et al., 2011; Noble et al., 2012, 2017; Wyatt et al., 2014; Roshan et al., 2015; Middag et

65 al., 2018). Such efforts have transformed our understanding of the biogeochemical processes

66 associated with Zn and Co cycling (Saito et al., 2017; Vance et al., 2017; Weber et al., 2018;

67 Tagliabue et al., 2018; Roshan et al., 2018) yet there are still geographically important regions

68 of the Atlantic that remain largely understudied, including the Southeast Atlantic.

69 The Sub-Tropical Front (STF) of the Southeast Atlantic represents the convergence of warm,

70 predominately macronutrient-limited Sub-Tropical Surface Water (STSW) and cold, iron-

71 limited but macronutrient enriched sub-Antarctic Surface Water (SASW), creating one of the

72 most dynamic nutrient regimes in the oceans (Ito et al., 2005; Browning et al., 2014; Moore,

73 2016). Here, the relative supply and availability of macronutrients and iron (Fe) exert an

74 important control in maintaining the elevated phytoplankton stock and productivity that is

75 typical of this frontal region, particularly during austral spring and summer (Moore and Abbott,

76 2000; Ito et al., 2005; Browning et al., 2014). Dissolved Zn is also depleted in SASW that flows

77 northwards to converge with STSW at the STF (Wyatt et al., 2014). However, the potential

78 role for Zn in the mediation of phytoplankton distribution and community structure in this

79 region is currently unclear.

80 Using data from two UK-GEOTRACES cruises (transect GA10) this study examines the

81 seasonal availability and ecological stoichiometry of dZn and dCo, by analysis of their

82 relationships with phosphate, in upper ocean waters of the Southeast Atlantic. These data,

83 together with measurements of phytoplankton pigment biomass and community structure, offer

84 an improved knowledge of the seasonal influences of external input and phytoplankton

85 succession on the distribution and cycling of Zn and Co in these dynamic waters.

86

87 **2.   Methods**

88 **2.1.   Sampling methods**

89 Seawater samples were collected during two UK-GEOTRACES cruises in the South Atlantic

90 Ocean (GA10, Fig. 1). The first cruise (D357) took place during austral spring 2010 (18th

91 October to 22nd November 2010), sampling the Southeast Atlantic on-board the *RSS*

92 *Discovery*. During D357, two transects were completed between Cape Town and the zero

93 meridian that represent early austral spring (D357-1) and late austral spring (D357-2),

94 respectively. The second cruise (JC068) took place during austral summer 2011/2012 (24th

95 December 2011 to 27th January 2012), along the same transect of the first cruise and continuing

96 along 40ºS between Cape Town and Montevideo, Uruguay, on-board the *RSS James Cook*. For

97 JC068, we present here only the repeat transect data between Cape Town and 13°W that

98 represents the Southeast Atlantic aspect of this transect. The stations occupied during the three

99 transects were not identical, but rather represent a coverage of the Southern Ocean and sub-

100 tropical waters present. Where stations were reoccupied during one or more transects, they

101 have the same station number.

102 All sampling bottles were cleaned according to the procedures detailed in the GEOTRACES

103 sample handling protocols (Cutter et al., 2010). Seawater and particulate samples below 15 m

104 depth were collected using a titanium-frame CTD with 24 trace metal clean 10 L Teflon-coated

105 OTE (Ocean Test Equipment) Niskin bottles deployed on a plasma rope. Sub-samples for

106 dissolved trace metal analysis were filtered through 0.8/0.2 µm cartridge filters (AcroPak^{TM}

107 500, Pall) into 125 mL low density polyethylene bottles inside a class 1000 clean air container.

108 Each sub-sample was acidified to pH 1.7 (0.024 M) by addition of 12 M hydrochloric acid

109 (HCl, UpA, Romil) under a class 100 laminar flow hood. Vertical sampling for dissolved trace

110 metals was augmented by surface samples collected at each station using a towed 'fish'

111 positioned at approximately 3-5 m depth. Fish samples were filtered in-line and acidified as

112 described for samples collected from the titanium sampling system. Particulate samples were

113 collected onto acid clean 25 mm, 0.45 µm, polyethersulfone membrane disc filters (Supor®,

114 Pall) and stored frozen (-20ºC) until shore-based analysis.

115

116 **2.2.   Trace metal analysis**

117 Dissolved Co was determined in the ISO accredited clean room facility (ISO 9001) at the

118 University of Plymouth (UK) using flow injection with chemiluminescence detection,

119 modified from the method of Cannizzaro et al. (1999) as described by Shelley et al. (2010).

120 Briefly, dCo was determined in UV-irradiated samples using the reaction between pyrogallol

121 (1,2,3-trihydrobenzene) and hydrogen peroxide formed in the presence of Co. Standards (20 –

122 120 pM Co) were prepared in 0.2 µm filtered low-dCo seawater (16.5 ± 5.2 pM, $n = 15$) by

123 serial dilution of a 1000 ppm Co ICP-MS standard (Romil, UK). The accuracy of the analytical

124 method was validated by quantification of dCo in SAFe (S and D2) and GEOTRACES (GD)

125   reference seawater (Table 1). There was no detectable analytical dCo blank and the limit of

126   detection (3σ of the lowest concentration standard) was 1.98 ± 0.87 pM ($n = 15$).

127   Dissolved Zn was determined using flow injection coupled with fluorescence detection,

128   modified from the method of Nowicki et al. (1994) and described previously for this

129   GEOTRACES section by Wyatt et al. (2014). The accuracy of the analytical method was

130   validated by quantification of dZn in SAFe (S and D2) reference seawater (Table 1). The blank

131   for dZn FIA was 0.14 ± 0.13 nM and the limit of detection (3σ of the lowest concentration

132   standard) was 0.01 ± 0.01 nM ($n = 15$).

133   Measurement uncertainties were estimated after the Nordtest approach (Worsfold et al., 2019)

134   where a combined uncertainty (u_c) is computed from day-to-day within-lab reproducibility and

135   uncertainties associated with the determination of reference materials (Table 1). This approach

136   creates higher uncertainties than those previously published for dZn and dCo analyses but

137   provides a more realistic estimation of analytical uncertainty. During this study, the u_c for dZn

138   and dCo analysis was 22 and 19 %, respectively, similar to the $13 - 25$ % reported by Rapp et

139   al. (2017) for the determination of trace metals, including dZn and dCo, by on-line pre-

140   concentration and high-resolution sector field ICP-MS detection. The elevated u_c within our

141   data results from the greater uncertainty surrounding the very low dZn and dCo concentration

142   SAFe S reference sample whereas the dZn and dCo u_c using only the Safe D2 are <5 %.

143   Hereafter, when presenting low dZn and dCo concentrations for comparison with

144   phytoplankton biological requirements (Section 3.5), we apply a fixed u_c of 20 % to our data.

145   Total particulate trace metals (i.e. pZn, pCo, pTi) were determined using inductively coupled

146   plasma-mass spectrometry (Thermo Fisher XSeries-2) following a sequential acid digestion

147   modified from Ohnemus et al. (2014). Potential interferences (e.g. $_{40}Ar_{16}O$ on $_{56}Fe$) were

148   minimized through the use of a collision/reaction cell utilizing 7 % H in He and evaluation of

149 efficiency and accuracy assessed using Certified Reference Material (CRM). Full details of the

150 method and CRM results can be found in Milne et al. (2017).

151

152 **2.3.   Nutrients, phytoplankton, temperature and salinity**

153 The dissolved macronutrients phosphate (PO_4^{3-}), silicic acid ($Si(OH)_4$ but referred to as Si

154 hereafter) and nitrate (determined as nitrate + nitrite, NO_3^-) were determined in all samples for

155 which trace metals were determined, in addition to samples collected from a stainless steel

156 rosette. Macronutrients were determined using an AA III segmented-flow AutoAnalyzer (Bran

157 & Luebbe) following colorimetric procedures (Woodward and Rees, 2001). Salinity,

158 temperature and depth were measured using a CTD system (Seabird 911+) whilst dissolved O_2

159 was determined using a Seabird SBE 43 O_2 sensor. Salinity was calibrated on-board using

160 discrete samples taken from the OTE bottles and an Autosal 8400B salinometer (Guildline)

161 whilst dissolved O_2 was calibrated using a photometric automated Winkler titration system

162 (Carritt and Carpenter, 1966). Mixed-layer depths (MLD) were calculated using the threshold

163 method of de Boyer Montégut et al. (2014), where MLD is identified from a linear interpolation

164 between near-surface density and the depth at which density changes by a threshold value

165 (0.125 kg m^{-3}).

166 Measurements of phytoplankton pigment biomass and community structure were made on

167 discrete samples collected using a 24 position stainless-steel CTD rosette equipped with 20 L

168 OTE Niskin bottles. For chlorophyll-*a* analysis, samples were filtered (0.7 µm Whatman GF/F)

169 and then the filters extracted overnight in 90 % acetone (Holm-Hansen et al., 1965). The

170 chlorophyll-*a* extract was measured on a pre-calibrated (spinach chlorophyll-*a* standard,

171 Sigma) Turner Designs Trilogy fluorometer. High performance liquid chromatography

172 (HPLC) samples (0.5 – 2 L) for accessory pigment analyses were filtered (0.7 µm Whatman

173 GF/F), flash frozen in liquid nitrogen and stored at -80 °C prior to analysis using a Thermo

174 HPLC system. The matrix factorization program CHEMTAX was used to estimate the

175 contribution of taxonomic groups to total chlorophyll-*a* (Mackey et al., 1996). Concentrations

176 of nanophytoplankton, *Synechococcus*, *Prochlorococcus* and photosynthetic picoeukaryotes

177 were analysed by analytical flow cytometry (AFC) using a FACSort flow cytometer (Becton

178 Dickenson, Oxford, UK) according to the methods described in Davey et al. (2008) and Zubkov

179 et al. (2003).

180

181 **3.   Results and Discussion**

182 **3.1.   Hydrographic setting and macronutrient distributions**

183 The prominent waters masses along the D357 and JC068 transects (Fig. 2) were identified by

184 their characteristic thermohaline and macronutrient properties (Sarmiento et al., 2004; Ansorge

185 et al., 2005; Browning et al., 2014). Wyatt et al. (2014) provide a more detailed description of

186 the JC068 hydrography along the entire GA10 section. Whilst we aim to compare the nearshore

187 versus offshore distributions of micro- and macronutrients, note that sub-Antarctic mode water

188 was not sampled for trace metals during the D357-2 late spring transect, and therefore only the

189 early spring and summer values are discussed for SASW hereafter.

190

191 *Surface mixed-layer*

192 During all three transects the STF was identified by a sharp potential temperature (θ) gradient

193 in the upper 200 m with the θ 15°C isotherm corresponding well to changes in macronutrient

194 concentrations between STSW and SASW. North of the STF, mixed-layer macronutrient

195 concentrations (Table 2) decreased in STSW between the three occupations of the transect. The

196 largest relative depletion observed was for NO_3^- with a ~2.7-fold reduction in mean inventory

197 concentration from 870 to 326 µmol m^{-3} between early spring and summer, whilst PO_4^{3-} and

198 Si concentrations were reduced 1.5- and 1.4-fold, respectively. The largest absolute depletion

199 was observed for Si with a reduction of 848 µmol m^{-3} between early spring and summer.

200 Conversely, summer SASW mixed-layer mean concentrations of NO$_3^-$, PO$_4^{3-}$ and Si were

201 relatively 1.6, 1.4 and 2.1-fold lower than early spring, respectively, whilst the largest absolute

202 depletion of 1912 µmol m^{-3} was observed for NO$_3^-$. SASW mixed-layer concentrations of NO$_3^-$

203 and PO$_4^{3-}$ were at least 2.1-fold higher than for STSW during the study, whilst the Si

204 concentration was at least 1.5-fold lower, highlighting the relative deficiencies in major

205 nutrients between high and low latitude derived surface waters (Sarmiento et al., 2004; Moore,

206 2016).

207

208 *Sub-surface waters*

209 The Southern Ocean derived Sub-Antarctic Mode Water (SAMW) and underlying Antarctic

210 Intermediate Water (AAIW) were identified using their characteristic core potential density

211 ($\sigma\theta$ 26.8 kg m^{-3}) (Sarmiento et al., 2004; Palter et al., 2010) and thermohaline (S <34.4, θ

212 >2.8ºC) properties (Fig. 2). Wyatt et al. (2014) have identified these water masses along this

213 section between 200 and 500 m. During all three transects, low sub-surface (50 − 500 m)

214 macronutrient concentrations were observed between 13 and 16°E, associated with a salinity

215 maxima. The feature conforms to the mean locality and depth range of Agulhas water

216 (Duncombe Rae, 1991), clearly highlighting the penetration of Indian Ocean water into

217 northward flowing SAMW.

218

219 **3.2.   Zn and Co distributions of the Southeast Atlantic Ocean**

220 *Surface mixed-layer*

221 Figure 3 shows the dZn and dCo distributions for the upper 500 m of the Southeast Atlantic for

222 the D357 and JCO68 transects. For full-depth dZn distributions along JC068 refer to Wyatt et

223 al. (2014). In the surface mixed-layer, dZn and dCo concentrations ranged from 0.01 to 4.57

nM and 1 to 50 pM, respectively. The large range in dZn concentrations resulted from an apparent offshore transport of elevated dZn within STSW between 20 – 50 m during early spring (1.48 – 4.57 nM; Stns. 1 – 2) that was reduced by late spring (0.48 – 1.76 nM; Stns. 0.5 – 1.5) and was absent during summer (0.01 – 0.13 nM; Stns. 1 – 2). Similarly, but to a lesser extent, elevated dCo concentrations were observed in STSW between 10 and 50 m during early and late spring (15 – 50 pM), compared with summer (18 – 33 pM). Our findings are consistent with previous observations of elevated dissolved and particulate trace metals over the same depth range in waters close to South Africa, including Co, Fe, Mn, and Pb (Chever et al., 2010; Bown et al., 2011; Boye et al., 2012; Paul et al., 2015). We postulate that these trace metal enrichments can arise from either atmospheric inputs, and/or from the lateral advection of metal-enriched waters from the Agulhas Current (AC) and/or South African continental shelf, and discuss this further in Sect. 3.3. In SASW, mixed-layer dZn and dCo concentrations ranged from 0.01 to 0.25 nM and 3 to 18 pM, respectively, during the study, significantly lower than STSW values, with the lowest concentrations observed during the summer transect (Table 2).

Sub-surface waters

During the early spring D357-1 transect, elevated dZn and dCo concentrations were observed between the surface mixed-layer and 500 m (1.48–3.85 nM and 39–62 pM, respectively) at the station closest the South African continent (Stn. 1). Here, the highest dZn concentrations were associated with the dZn-enriched waters (20–55 m) described above for the surface mixed-layer. During the late spring D357-2 transect, the near-shore (Stns. 0.5–1) dZn concentrations were lower (0.31–1.76 nM) whilst dCo remained similar to early spring values (27–57 pM). During summer, near-shore (Stn. 1) sub-surface dZn concentrations were markedly lower (0.03–0.50 nM) than spring values whilst dCo concentrations (17–52 pM) were only marginally lower. In offshore waters, sub-surface dZn concentrations ranged from 0.01 to 1.01

249   nM across all three transects with extremely low values in the upper 400 m (0.22 ± 0.21 nM)

250   and the highest values between 400 and 500 m. The absence of a significant return path for

251   dZn with SAMW to waters above 400 m at this latitude (Wyatt et al., 2014; Vance et al., 2017)

252   is likely an important control on dZn distributions across all three transects. In contrast, dCo

253   concentrations were depleted in the upper 200 m (1–35 pM) and elevated in SAMW (23–56

254   pM) suggesting that these Southern Ocean derived waters also play an important role in upper

255   water column dCo distributions of the South Atlantic.

256   To assess whether seasonal changes in subsurface supply could influence dissolved Zn and Co

257   concentrations in the upper water column of the Southeast Atlantic, we examined the metal

258   versus PO_4^{3-} distributions of underlying SAMW and AAIW. Throughout this paper metal:PO_4^{3-}

259   will be used to indicate an uptake remineralisation ratio derived from a regression slope, whilst

260   metal/PO_4^{3-} will denote a concentration ratio. Figure 4 and supplementary table 1 show how

261   the dZn:PO_4^{3-} regression slope for SAMW and AAIW varied little between the three transects.

262   These slopes are a function of the pre-formed micro- and macronutrient concentrations and the

263   uptake/remineralisation ratio of the sources waters, as well as mixing during advection between

264   the Southern Ocean and South Atlantic (Vance et al., 2017; Middag et al., 2018). The dZn:PO_4^{3-}

265   slopes steepen with the introduction of AAIW with higher dZn/PO_4^{3-} concentration ratios, yet

266   it is the relatively shallow slopes of overlying SAMW that imply a low, and relatively

267   consistent, subsurface supply of dZn to STSW and SASW of the South Atlantic (Wyatt et al.,

268   2014). The shallower waters overlying SAMW clearly show elevated dZn concentration,

269   specifically during the spring transects, compared with what could be delivered if subsurface

270   supply was the dominant source governing dZn availability in surface waters (Fig. 4). It is

271   therefore unlikely that a change in subsurface supply from underlying SAMW is responsible

272   for the change in dZn inventories of STSW and SASW between the three transects.

273   Similarly, the dCo:PO_4^{3-} regression slope varied little between the three transects (Fig. 4 and

274   Supp. Table 1). In dCo:PO_4^{3-} space, a single slope can be fit to SAMW and AAIW with no net

275   scavenging effect on dCo distribution over the upper 1000 m. Like dZn, the waters overlying

276   SAMW displayed spring dCo concentrations elevated above that potentially delivered via

277   SAMW supply. During summer however, SAMW may provide a subsurface source of dCo

278   (Fig. 4c) to overlying waters highlighting how Southern Ocean derived waters may play

279   important, yet different, roles in upper water column metal distributions of the Southeast

280   Atlantic.

281

3.3.   Shelf derived sources of Zn and Co

283   Potential sources of trace metals to surface waters of the Southeast Atlantic include

284   atmospheric inputs from South Africa and Patagonia (Chance et al., 2015; Menzel Barraqueta

285   et al., 2019) as well as interactions with shelf and slope waters of the Agulhas Bank (Bown et

286   al., 2011; Boye et al., 2012; Paul et al., 2015). During the D357 spring transects, elevated

287   mixed-layer dZn and dCo concentrations (up to 4.57 nM and 50 pM, respectively; Sect. 3.2)

288   were observed at stations closest the Agulhas Bank shelf and slope (Stns. 0.5, 1, 1.5 and 2).

289   Here, we compare these metal elevations with respect to the aforementioned sources. Firstly,

290   we encountered only brief, light rain during the study, thus minimal wet deposition of

291   atmospheric aerosol. By combining the median atmospheric dry deposition flux for soluble Zn

292   and Co for the Southeast Atlantic (Zn 6.0 and Co 0.05 nmol m^{-2} d^{-1}; Chance et al., 2015) with

293   the mean mixed-layer depth (34 m) for STSW during D357, dust dissolution is estimated to

294   add approximately 5.5 and 0.05 nmol m^{-3} dZn and dCo, respectively, over a one month period.

295   These inputs are low compared with the mixed-layer metal inventories, representing <1 % of

296   dZn and dCo concentration in STSW during the D357 transects (Table 2), and would not be

297   sufficient to generate distinct mixed-layer maxima. It is likely, therefore, that the dZn and dCo

298 elevations originated from the advection of metal-enriched waters from the western Agulhas

299 Bank, a region identified as a distinct source of both dissolved and particulate trace metals to

300 the Southeast Atlantic (Chever et al., 2010; Bown et al., 2011; Boye et al., 2012; Paul et al.,

301 2015), and/or from the leakage of Indian Ocean water into the Southeast Atlantic via the AC.

302 The detachment of Agulhas rings and filaments from the AC during its retroflection back

303 towards the Indian Ocean constitutes a source of Pb to the surface Southeast Atlantic along the

304 D357 transects (Paul et al., 2015). Whilst we observed elevated mixed-layer dZn and dCo at

305 ~15ºE during both D357 transects, the absence of metal enrichment across the depth of the AC

306 salinity maxima (Figs. 2 and 3) suggests that the signal must be entrained from elsewhere.

307 Furthermore, dZn concentrations from the AC along the east coast of South Africa do not

308 exceed 0.5 nM in the upper 200 m (Gosnell et al., 2012). It is therefore likely that the dZn and

309 dCo enrichment was derived from the Agulhas Bank. The AC has been shown to meander over,

310 and interact with, the Agulhas Bank, forming eddies and filaments on the shoreward edge of

311 the AC proper, that tend to move northwards along the western shelf edge and into the

312 Southeast Atlantic (Lutjeharms and Cooper, 1996; Lutjeharms, 2007), potentially delivering

313 shelf-derived sedimentary material. We found no evidence of a fluvial signature in our data,

314 and no significant fluvial source for trace elements to our study region has been reported in the

315 literature. We focus here on the more likely scenario of sedimentary inputs as the driver of

316 mixed-layer dZn and dCo elevations at the shelf and slope stations during D357. Despite no

317 available particulate trace metal data for the D357-1 early spring transect for direct comparison

318 with the highest dZn and dCo elevations, we observed elevated mixed-layer particulate Zn

319 (pZn; 0.08–1.40 nM) and Co (pCo; 8–49 pM) at stations closest South Africa during the D357-

320 2 late spring transect (Stns. 0.5, 1 and 1.5, Fig. S1), coincident with elevated dZn (0.05–1.82

321 nM) and dCo (1–43 pM). Furthermore, for the upper 500 m at stations 0.5 and 1, we found

322 strong positive correlations between particulate aluminium and titanium (pAl:pTi, slope 41.7

323 mol mol^{-1}, Pearson's r 0.99, $n = 15$), as well as particulate Fe and titanium (pFe:pTi, slope 10.2

324 mol mol^{-1}, Pearson's r 0.99, $n = 15$), indicative of a strong lithogenic source. Whilst there are

325 presently no South African sedimentary data against which we can compare our water column

326 values, our pAl:pTi and pFe:pTi slope ratios are in excess of upper crustal mole ratios (34.1

327 and 7.3 mol mol^{-1}, respectively; Mclennan, 2001). These 500 m ratios are also steeper than the

328 aggregate slopes for the full depth Atlantic Ocean away from hydrothermal sources (32.1 and

329 7.4 mol mol^{-1}, Pearson's r >0.97, $n = 593$, Schlitzer, 2018). Given the refractory nature of

330 lithogenic pTi across diverse oceanic environments (Ohnemus and Lam, 2015), this may

331 suggest the resuspension and dissolution of Agulhas Bank sediments enriched in dAl and dFe,

332 followed by westward offshore transport, a common feature of the Bank's physical circulation

333 during spring and summer (Largier et al., 1992). Such processes may in turn provide an

334 additional source of dZn and dCo to STSW of the Southeast Atlantic. For example, Little et al.

335 (2016) proposed that oxygen-deficient, organic-rich, continental margin sediments may

336 constitute a significant global sink within the marine Zn cycle. These sediments could

337 additionally provide a local source of dZn following remineralisation. Recent model outputs

338 have likewise highlighted oxygen-deficient, boundary sediments as a dominant external source

339 of Co to the oceans (Tagliabue et al., 2018). Given that oxygen depleted (<45 µM) bottom

340 waters are prevalent across the western Agulhas Bank (Chapman and Shannon, 1987;

341 Chapman, 1988), considered to arise from high organic matter input to sediments and its

342 bacterial decomposition, a sedimentary source of dZn and dCo appears likely.

343

344 **3.4.   Trace metal stoichiometry of the upper Southeast Atlantic**

345 In addition to seasonal variations in the lateral advection of continentally derived trace metals,

346 the lower dZn and dCo concentrations in STSW during summer, compared with spring, likely

347 reflect differences in biological utilisation. Here, we examine the micro- and macronutrient

348 concentration inventories to assess the trace metal stoichiometry of the Southeast Atlantic over

349 seasonal timescales. The data were grouped into STSW and SASW regimes, with STSW

350 defined by $\theta \geq 15°C$. This isotherm was located at a mean depth of 144 ± 96 m across the study,

351 compared with a mean mixed-layer depth of 39 ± 10 m, and thus the inventories for SASW

352 were determined over this depth for comparison with STSW (Table 2). Early and late spring

353 STSW samples in the depth range 20 - 55 m that clearly exhibited continentally derived

354 elevated dZn and dCo were removed from the analysis in order to compare stoichiometry with

355 respect to biological processes. For SASW, micronutrient sampling did not occur during late

356 spring and therefore only early spring and summer values are compared.

357 Distinct temporal trends in the stoichiometric relationship with PO_4^{3-} were evident for both dZn

358 and dCo (Fig. 4). Within STSW, the dZn/PO_4^{3-} inventory ratio ranged from 699 to 1876 µmol

359 mol^{-1} (Table 2) with the highest value observed during early spring and the lowest during

360 summer. Combined with summer dZn concentrations 4-fold lower than early spring, this

361 suggests strong biological uptake of dZn alongside PO_4^{3-} between seasons. In contrast, lower

362 dZn/PO_4^{3-} ratios of 372 and 188 µmol mol^{-1} were observed in SASW during early spring and

363 summer, respectively. Here, the absolute change in dZn concentration between spring and

364 summer was lower than for STSW, but was greater for PO_4^{3-}, likely reflecting the increased

365 availability of PO_4^{3-} in these Southern Ocean derived waters (Table 2) and an open-ocean

366 phytoplankton community that have lower trace metal requirements than their counterparts

367 north of the STF. Such dZn/PO_4^{3-} ratios sit at the lower end of cellular Zn/P reported for the

368 diatom and haptophyte-type phytoplankton typical of this region (~100 – 1100 µmol mol^{-1};

369 Twining and Baines, 2013 and refs. therein), highlighting the importance of micronutrient

370 processes with respect to Zn availability.

371 In contrast to dZn, the spatiotemporal variation observed for STSW dCo/PO_4^{3} was small with

372 ratios ranging from 82 to 129 µmol mol^{-1} (Table 2), likely reflecting external inputs to the

oceans and biological Co requirements that are typically 4-fold less than for Zn (Ho et al., 2003; Roshan et al., 2016; Hawco et al., 2018). The STSW dCo/PO_4^{3-} ratio decreased between early and late spring transects, potentially in part due to the westward expansion of STSW during late spring (Fig. 2) and subsequent mixing with SASW depleted in dCo relative to PO_4^{3-} (Fig. 3). This dilution is likely also true of dZn and Si, yet their STSW concentration inventories may be sufficiently high as to mask this effect. Unfortunately, an insufficient quantity of late spring SASW data are available with which to affirm this postulation. The highest dCo/PO_4^{3-} ratio was observed during summer due to the preferential biological removal of PO_4^{3-} relative to dCo.

In SASW, dCo/PO_4^{3-} was consistently low with ratios of 23 and 26 µmol mol^{-1} for early spring and summer, respectively. Much higher inventory ratios of ~580 µmol mol^{-1} can be calculated over similar depths for open-ocean North Atlantic waters (GA03 Stns. 11-20, Schlitzer et al., 2018), likely reflecting an elevated atmospheric Co input and/or an extremely low surface PO_4^{3-} inventory (Wu et al., 2000; Martiny et al., 2019).

Our results provide evidence for the greater availability and preferential removal of dZn relative to dCo in the upper water column the Southeast Atlantic based on STSW dZn/dCo inventory ratios of 19, 17 and 5 mol mol^{-1} for the three transects and SASW ratios of 13 and 7 mol mol^{-1} for early spring and summer, respectively (Table 2). With relatively consistent inter-seasonal dCo inventories for STSW and SASW, indicating a more balanced ecophysiological regime with regard to dCo organisation, the change in dZn/dCo inventory stoichiometries principally reflects changes in dZn concentration. We postulate that the inter-seasonal variations in dZn and dCo availability and stoichiometry of the Southeast Atlantic reflect changes in the relative nutritional requirement of resident phytoplankton and/or biochemical substitution of Zn and Co to meet nutritional demand.

3.5.   Phytoplankton controls on trace metal ecological stoichiometry

Here we discuss the principle phenomena that together likely explain our observations of seasonally decreasing dZn/dCo inventory stoichiometries in STSW and SASW of the Southeast Atlantic: i.e. the preferential removal of dZn, relative to dCo, leading to low dZn availability, and differences in phytoplankton assemblages with different cellular metal requirements.

Satellite images show elevated surface chlorophyll concentrations across the Southeast Atlantic STF, compared with waters further north and south, with peak concentrations observed during summer in January 2012 (Fig. 1). Profiles of total chlorophyll-*a* concentration (Fig. S2) also show maximum summer values in the upper water column of STSW (1.02 mg m^{-3}) and SASW (0.49 mg m^{-3}) compared with spring values (<0.61 and <0.36 mg m^{-3}, respectively). This is consistent with the hypothesis that increasing irradiance, coupled with shallower mixed-layer depths (de Boyer Montégut et al., 2004), result in enhanced growth conditions across the STF between September and February (Browning et al., 2014). Diagnostic pigment analyses (Fig. 5a) indicated that eukaryotic nanophytoplankton, specifically *Phaeocystis*-type haptophytes, dominated the early spring STSW chlorophyll-*a* content (73 %) but with a reduced contribution during summer (20 %). Maximum growth rates for cultured *Phaeocystis antarctica* have been achieved under elevated Zn concentrations (Saito and Goepfert, 2008), and thus, the dominance of this haptophyte would likely contribute to the removal of dZn between spring and summer. Furthermore, an increased summer diatom contribution (13 % chlorophyll-*a* compared with near zero during spring transects) would have further reduced the dZn inventory, with diatoms having at least 4-fold higher cellular Zn/P ratios than co-occurring cell types (Twining and Baines, 2013).

The fact that both *Phaeocystis* and diatomaceous nanophytoplankton maintain a contribution to the summer STSW chlorophyll-*a* complement, when dZn availability is low, is intriguing.

423 Both *P. antarctica* and the large, coastal diatoms *Thalassiosira pseudonana* and *Thalassiosira*

424 *weissflogii* have been shown to be growth limited in culture by free Zn^{2+} concentrations ≤ 10

425 pM (Sunda and Huntsman, 1992; Saito and Goepfert, 2008). A simple estimate of summer

426 STSW free Zn^{2+} availability, based on North Atlantic organic complexation data (>96 %;

427 Ellwood and Van den Berg, 2000), indicated free Zn^{2+} averaged $6.3 \pm 5.3u_c$ pM, suggesting the

428 potential for growth limitation of these phytoplankton. In addition, when comparing the

429 Southeast Atlantic dZn stoichiometry with the cellular requirements of phytoplankton grown

430 under growth rate limiting conditions (Fig. 6), we found summer STSW dZn/PO_4^{3-} to be in

431 deficit of the requirements of coastal *T. pseudonana* but not those of the smaller, open-ocean

432 diatom *T. oceanica*. The variation in cellular Zn/P between small and large phytoplankton is

433 related to the higher surface-area-to-volume ratio of smaller cells, and the limitation of

434 diffusive uptake rates at low Zn^{2+} concentrations (Sunda and Huntsman, 1995). This would

435 suggest that the lower dZn availability in summer STSW should influence phytoplankton

436 species composition by selecting for smaller organisms with lower cellular Zn requirements,

437 and confirmed by a ratio of picophytoplankton to nanophytoplankton at least 4-fold higher

438 during summer compared with spring values. The comparison further implies that the presence

439 of *Phaeocystis* and diatoms in summer STSW may be linked with their metabolic Zn-Co-Cd

440 substitution capability, potentially allowing them to overcome some portion of their Zn

441 deficiency. Largely connected to carbonic anhydrase enzymes, several species of eukaryotic

442 phytoplankton are capable of biochemical substitution of Zn, Co or Cd to maintain optimal

443 growth rates under low trace metal conditions (Price and Morel, 1990; Sunda and Huntsman,

444 1995; Lee and Morel, 1995; Lane and Morel, 2000; Xu et al., 2007; Saito and Goepfert, 2008;

445 Kellogg et al., 2020). For example, metabolic substitution of Co in place of Zn has been

446 observed to support the growth of *P. antarctica*, *T. pseudonana* and *T. weissflogii* in media

447 with Zn^{2+} <3 pM (Sunda and Huntsman, 1995; Saito and Goepfert, 2008; Kellogg et al., 2020).

448   Thus, the lower mixed-layer dCo inventory of summer STSW, relative to early spring, may be

449   in part related to enhanced dCo uptake through biochemical substitution alongside the growth

450   of phytoplankton with distinct Co requirements.

451   In contrast to *Phaeocystis*, *E. huxleyi*-type haptophytes were near-absent in spring STSW (<5

452   % chlorophyll-*a*; Fig. 5a) and increased in contribution during summer (18 %). *Emiliania*

453   *huxleyi* appear to have a biochemical preference for Co over Zn (Xu et al., 2007), which could

454   potentially be a contributing factor to the increased fraction of this haptophyte in summer

455   STSW. Based on Co organic complexation data for Southeast Atlantic STSW (>99 %; Bown

456   et al., 2012), however, even the maximum dCo concentration of 56 pM (estimated free Co^{2+}

457    $0.56 \pm 0.11 u_c$ pM) observed for STSW during this entire study would limit the growth of

458   cultured *E. huxleyi* in the absence of Zn or Cd (Sunda and Huntsman, 1995; Xu et al., 2007).

459   This is supported by inter-seasonal dCo/PO_4^{3-} stoichiometries in deficit of the cellular

460   requirements of cultured *E. huxleyi* (Fig. 6). Despite this, Xu et al. (2007) showed that *E.*

461   *huxleyi* can maintain significant growth at only 0.3 pM Co^{2+} in the presence of Zn, with the

462   limitation by, and substitution of these metals reported to occur over a range of free ion

463   concentrations (0.2–5 pM) that is relevant to summer conditions of the Southeast Atlantic. This

464   assessment implies an additional need for Zn in phytoplankton nutrition due to low dCo

465   availability throughout the Southeast Atlantic, which may accelerate the decrease in dZn/dCo

466   inventory ratio between seasons.

467   The elevated summer STSW chlorophyll-*a* concentrations were accompanied by increased cell

468   concentrations of the *Synechococcus* and *Prochlorococcus* (up to 100 and 400 cells μL^{-1},

469   respectively) relative to early spring abundance (Fig. 5b). This pattern suggests an inter-

470   seasonal community shift towards smaller picocyanobacterial cells that is coincident with

471   decreased dZn availability. *Synechococcus* and *Prochlorococcus* are thought to have little or

472   no Zn requirement and relatively low Co requirements (growth limited by ≤0.2 pM Co^{2+}; Sunda

473 and Huntsman, 1995; Saito et al., 2002). This, alongside their small cell size, hence greater

474 capacity for acquiring fixed nitrogen under conditions where this nutrient is depleted, may

475 allow these prokaryotes to flourish following depletion and export of Zn associated with

476 *Phaeocystis* and diatom blooms. This supposition is supported by a persistently high abundance

477 of *Synechococcus* and *Prochlorococcus* (>1000 cells μL^{-1}), relative to eukaryotic

478 nanophytoplankton, in the dZn depleted surface waters of the Costa Rica Dome (Saito et al.,

479 2005; Ahlgren et al., 2014; Chappell et al., 2016). Here, surface dCo concentrations were

480 maintained above that of surrounding waters by the biological production of Co-binding

481 ligands (Saito et al., 2005). The increased abundance of these prokaryotic autotrophs in summer

482 STSW of the Southeast Atlantic may have also contributed to the inter-seasonal decrease in

483 dCo inventory.

484 In contrast to STSW, cells counts of eukaryotic phytoplankton and prokaryotic cyanobacteria

485 in SASW varied little between early spring and summer (Fig. 5b), indicative of a more balanced

486 ecophysiological regime. The fractional contribution of *Phaeocystis* (Fig. 5a), the dominant

487 contributor to the SASW chlorophyll-*a* complement, was similar between transects at 54 and

488 44 %, respectively, whilst the contribution of *E. huxleyi* increased from 19 to 33 % between

489 spring and summer, respectively. Whilst it is proposed that the low Fe supply rate to these

490 waters provides a dominant control on phytoplankton biomass and composition (Browning et

491 al., 2014), low dZn and dCo availability may also be important drivers of such change. The

492 Summer SASW dZn inventory (0.08 ± 0.07u_c nM) and stoichiometry with PO_4^{3-} (Fig. 6)

493 indicate growth limiting conditions for *Phaeocystis* and *E. huxleyi* in the absence of

494 cambialistic metabolism (Sunda and Huntsman., 1995; Saito and Goepfert, 2008; Xu et al.,

495 2007). The presence of these phytoplankton therefore indicates Zn biochemical substitution

496 occur in oceanic waters of the Southeast Atlantic. A lower Co half-saturation growth constant

497 for cultured *P. antarctica* (K_m = ~0.2 pM Co^{2+}), compared with *E. huxleyi* (K_m = ~3.6 pM

498   Co^{2+}), further suggests that *Phaeocystis* species may more effectively occupy low dZn and dCo

499   environments (Saito and Goepfert, 2008), such as SASW of the South Atlantic.

500   Conversely, the absence of a significant diatom contribution to summer SASW chlorophyll-*a*

501   (Fig. 5a), relative to early spring, is surprising as the summer dZn/PO_4^{3-} inventory ratio is in

502   excess of the cellular Zn/P requirements of typical oceanic diatoms such as *T. oceanica* (Fig.

503   6). Furthermore, whilst the dCo/PO_4^{3-} ratio of summer SASW is in deficit of the cellular Co/P

504   below which growth limitation of *T. oceanica* may occur, this species has been shown to grow

505   effectively at Co^{2+} <0.1 pM in culture in the presence of Zn (Sunda and Huntsman, 1995). The

506   low diatom fractional contribution to summer SASW may be instead related to low Fe

507   availability (Browning et al., 2014) and stress-induced Si exhaustion. In support of this, we

508   calculate summer SASW mixed-layer Si concentrations (0.9 ± 0.3 µM) to be 50 % of early

509   spring values (1.8 ± 0.2 µM) with a dissolved NO_3^-/Si stoichiometry of 3.8 mol mol^{-1} close to

510   the 4 mol mol^{-1} shown to limit diatom growth in culture (Gilpin et al., 2004), and in contrast to

511   the 2.9 mol mol^{-1} calculated for early spring.

512

3.6.   Conclusion

514   We report the distributions of dZn and dCo in the upper water column of sub-tropical and sub-

515   Antarctic waters of the Southeast Atlantic during austral spring and summer periods. We

516   identify an apparent continental source of dZn and dCo to sub-tropical waters at depths between

517   20 − 55 m, derived from sedimentary inputs from the Agulhas Bank. In contrast, open-ocean

518   sub-Antarctic surface waters displayed largely consistent inter-seasonal mixed-layer dZn and

519   dCo concentrations indicating a more balanced ecophysiological regime with regard to their

520   organisation. The vertical distributions of dZn and dCo in the upper water column were similar

521   to that of PO_4^{3-} indicating biological drawdown in surface waters and mixing with underlying

522   Southern   ocean-derived   waters   travelling   equatorward   significantly   influences   their

523 distribution. Absolute trace metal concentrations alongside concentration inventory ratios

524 suggest the preferential utilization of dZn, relative to dCo, in the Southeast Atlantic with

525 dZn/dCo decreasing from 19 to 5 mol mol^{-1} between early spring and summer in STSW and

526 from 13 to 7 mol mol^{-1} in SASW. This pattern is consistent with our understanding of the

527 cellular requirement of phytoplankton (Twining and Baines, 2013). The inter-seasonal removal

528 of dZn results in summer concentrations that are potentially growth limiting for certain

529 phytoplankton species estimated to be present in these waters by diagnostic pigment analyses.

530 We therefore suggest cambialistic metabolic substitution between Zn and Co, and potentially

531 Cd, is an important factor regulating the growth, distribution and diversity of phytoplankton in

532 the Southeast Atlantic.

533

534 *Data availability.* The trace metal and macronutrient data sets used for analyses in this study

535 are available at https://www.bodc.ac.uk/geotraces/data/idp2017/ (GEOTRACES GA10) and

536 phytoplankton data at https://www.bodc.ac.uk/.

537

538 *Competing interests.* The authors declare that they have no conflict of interest.

539

540 *Author contribution.* MCL and EPA acquired the funding. NJW, MCL, AM, TJB, EMSW, and

541 HAB collected samples at sea. NJW conducted the Zn and Co measurements, EMSW the

542 macronutrient measurements and TJB the phytoplankton measurements. NJW prepared the

543 manuscript with significant contributions from all co-authors.

544

545 *Acknowledgments.* We thank the officers, crew, technicians and scientists of the *RRS James*

546 *Cook* for their help on the UK-GEOTRACES D357 and JC068 cruises. This work was funded

547 by the UK-GEOTRACES National Environmental Research Council (NERC) Consortium

548 Grant (NE/H006095/1 (MCL & HAB) & NE/H004475/1 (EPA)).

549

550 References

551 Ahlgren, N. A., Noble, A. E., Patton, A. P., Roache-Johnson, K., Jackson, L., Robinson, D.,
552 McKay, C., Moore, L. R., Saito, M. A., and Rocap, G.: The unique trace metal and mixed layer
553 conditions of the Costa Rica upwelling dome support a distinct and dense community of
554 Synechococcus, Limnol. Oceanogr., 59, 2166-2184, doi:10.4319/lo.2014.59.6.2166, 2014.

555 Ansorge, I. J., Speich, S., Lutjeharms, J. R. E., Goni, G. J., Rautenbach, C. J. D., Froneman, P.
556 W., Rouault, M., and Garzoli, S.: Monitoring the oceanic flow between Africa and Antarctica:
557 Report of the first Goodhope cruise, S. Afr. J. Sci., 101, 29-35, 2005.

558 Bertrand, E. M., Saito, M. A., Rose, J. M., Riesselman, C. R., Lohan, M. C., Noble, A. E., Lee,
559 P. A., and DiTullio, G. R.: Vitamin b12 and iron colimitation of phytoplankton growth in the
560 Ross Sea, Limnol. Oceanogr., 52, 1079-1093, doi:10.4319/lo.2007.52.3.1079, 2007.

561 Bown, J., Boye, M., Baker, A., Duvieilbourg, E., Lacan, F., Le Moigne, F., Planchon, F.,
562 Speich, S., and Nelson, D. M.: The biogeochemical cycle of dissolved cobalt in the Atlantic
563 and the Southern Ocean south off the coast of South Africa, Mar. Chem., 126, 193-206,
564 doi:10.1016/j.marchem.2011.03.008, 2011.

565 Bown, J., Boye, M., and Nelson, D. M.: New insights on the role of organic speciation in the
566 biogeochemical cycle of dissolved cobalt in the southeastern Atlantic and the Southern Ocean,
567 Biogeosciences, 9, 2719–2736, doi:10.5194/bg-9-2719-2012, 2012.

568 Boye, M., Wake, B. D., Garcia, P. L., Bown, J., Baker, A. R., and Achterberg, E. P.:
569 Distributions of dissolved trace metals (Cd, Cu, Mn, Pb, Ag) in the southeastern Atlantic and
570 the Southern Ocean, Biogeosciences, 9, 3231-3246, doi:10.5194/bg-9-3231-2012, 2012.

571 Browning, T. J., Bouman, H. A., Moore, C. M., Schlosser, C., Tarran, G. A., Woodward, E.
572 M. S., and Henderson, G. M.: Nutrient regimes control phytoplankton ecophysiology in the
573 South Atlantic, Biogeosciences, 11, 463-479, doi:10.5194/bg-11-463-2014, 2014.

574 Browning, T. J., Achterberg, E. P., Rapp, I., Engel, A., Bertrand, E. M., Tagliabue, A., and
575 Moore, C. M.: Nutrient co-limitation at the boundary of an oceanic gyre, Nature, 551, 242-246,
576 doi:10.1038/nature24063, 2017.

577 Cannizzaro, V., Bowie, A.R., Sax, A., Achterberg, E. P., Worsfold, P. J.: Determination of
578 cobalt and iron in estuarine and coastal waters using flow injection with chemiluminescence
579 detection, Analyst, 125, 51-57, doi:10.1039/A907651d, 2000.

580 Carritt, D. E., and Carpenter, J. H.: Comparison and evaluation of currently employed
581 modifications of the Winkler method for determining dissolved oxygen in seawater; a nasco
582 report, J. Mar. Res., 24, 286 - 319, 1966.

583 Chance, R., Jickells, T. D., and Baker, A. R.: Atmospheric trace metal concentrations,
584 solubility and deposition fluxes in remote marine air over the south-east Atlantic, Mar. Chem.,
585 177, 45-56, doi:10.1016/j.marchem.2015.06.028, 2015.

586 Chapman, P.: On the occurrence of oxygen-depleted water south of Africa and its implications
587 for Agulhas-Atlantic mixing, S. Afr. J. Marine Sci., 7, 267-294,
588 doi:10.2989/025776188784379044, 1988.

589 Chapman, P., and Shannon, L. V.: Seasonality in the oxygen minimum layers at the extremities
590 of the Benguela system, S. Afr. J. Marine Sci., 5, 85-94, doi:10.2989/025776187784522162,
591 1987.

592 Chappell, P. D., Vedmati, J., Selph, K. E., Cyr, H. A., Jenkins, B. D., Landry, M. R., and
593 Moffett, J. W.: Preferential depletion of zinc within Costa Rica upwelling dome creates
594 conditions for zinc co-limitation of primary production, J. Plankton Res., 38, 244-255,
595 doi:10.1093/plankt/fbw018, 2016.

596 Chever, F., Bucciarelli, E., Sarthou, G., Speich, S., Arhan, M., Penven, P., and Tagliabue, A.:
597 Physical speciation of iron in the Atlantic sector of the Southern Ocean along a transect from
598 the subtropical domain to the Weddell Sea Gyre, J. Geophys. Res-Oceans, 115, C10059,
599 doi:10.1029/2009jc005880, 2010.

600 Cox, A., and Saito, M.: Proteomic responses of oceanic Synechococcus WH8102 to phosphate
601 and zinc scarcity and cadmium additions, Front Microbiol, 4, doi:10.3389/fmicb.2013.00387,
602 2013.

603 Cullen, J. T., and Sherrell, R. M.: Effects of dissolved carbon dioxide, zinc, and manganese on
604 the cadmium to phosphorus ratio in natural phytoplankton assemblages, Limnol. Oceanogr.,
605 50, 1193-1204, doi:10.4319/lo.2005.50.4.1193, 2005.

606 Davey, M., Tarran, G. A., Mills, M. M., Ridame, C., Geider, R. J., and LaRoche, J.: Nutrient
607 limitation of picophytoplankton photosynthesis and growth in the tropical North Atlantic,
608 Limnol. Oceanogr., 53, 1722–1733, doi:10.4319/lo.2008.53.5.1722, 2008

609 de Boyer Montégut, C., Madec, G., Fischer, A. S., Lazar, A., and Iudicone, D.: Mixed layer
610 depth over the global ocean: An examination of profile data and a profile-based climatology,
611 J. Geophys. Res-Oceans, 109, C12003, doi:10.1029/2004jc002378, 2004.

612 Dulaquais, G., Boye, M., Middag, R., Owens, S., Puigcorbe, V., Buesseler, K., Masqué, P.,
613 Baar, H. J., and Carton, X.: Contrasting biogeochemical cycles of cobalt in the surface western
614 Atlantic Ocean, Global Biogeochem. Cy., 28, 1387–1412, doi:10.1002/2014GB004903, 2014.

615 Duncombe Rae, C. M.: Agulhas retroflection rings in the South Atlantic Ocean: An overview,
616 S. Afr. J. Marine Sci., 11, 327-344, doi:10.2989/025776191784287574, 1991.

617 Ellwood, M. J., and Van den Berg, C. M. G.: Zinc speciation in the Northeastern Atlantic
618 Ocean, Mar. Chem., 68, 295-306, doi:10.1016/S0304-4203(99)00085-7, 2000.

619 Franck, V. M., Bruland, K. W., Hutchins, D. A., and Brzezinski, M. A.: Iron and zinc effects
620 on silicic acid and nitrate uptake kinetics in three high-nutrient, low-chlorophyll (HNLC)
621 regions, Mar. Ecol. Prog. Ser., 252, 15-33, doi:10.3354/meps252015, 2003.

Gilpin, L. C., Davidson, K., and Roberts, E.: The influence of changes in nitrogen: silicon ratios on diatom growth dynamics, J. Sea Res., 51, 21-35, doi:10.1016/j.seares.2003.05.005, 2004.

Gosnell, K. J., Landing, W. M., and Milne, A.: Fluorometric detection of total dissolved zinc in the southern Indian Ocean, Mar. Chem., 132, 68-76, doi:10.1016/j.marchem.2012.01.004, 2012.

Hawco, N. J., and Saito, M. A.: Competitive inhibition of cobalt uptake by zinc and manganese in a Pacific Prochlorococcus strain: Insights into metal homeostasis in a streamlined oligotrophic cyanobacterium, Limnol. Oceanogr., 63, 2229-2249, doi:10.1002/lno.10935, 2018.

Hawco, N.J., Lam, P.J., Lee, J.M., Ohnemus, D.C., Noble, A.E., Wyatt, N.J., Lohan, M.C., and Saito M.A.: Cobalt scavenging in the mesopelagic ocean and its influence on global mass balance: synthesizing water column and sedimentary fluxes, Mar. Chem., 201, 151-166, doi.org/10.1016/j.marchem.2017.09.001, 2018.

Ho, T. Y., Quigg, A., Finkel, Z. V., Milligan, A. J., and Wyman, K.: The elemental composition of some marine phytoplankton, J. Phycol., 39, 1145-59, doi.org/10.1111/j.0022-3646.2003.03-090.x.

Holm-Hansen, O., Lorenzen, C. J., and Holmes, J. D. H.: Fluorometric determination of chlorophyll, ICES J. Mar. Sci., 30, 3-15, doi.org/10.1093/icesjms/30.1.3, 1965.

Ito, T., Parekh, P., Dutkiewicz, S., and Follows, M. J.: The Antarctic circumpolar productivity belt, Geophys. Res. Lett., 32, L13604, doi:10.1029/2005gl023021, 2005.

Jakuba, R. W., Moffett, J. W., and Dyhrman, S. T.: Evidence for the linked biogeochemical cycling of zinc, cobalt, and phosphorus in the western north Atlantic Ocean, Global Biogeochem. Cy., 22, GB4012, doi:10.1029/2007GB003119, 2008.

Jakuba, R. W., Saito, M. A., Moffett, J. W., and Xu, Y.: Dissolved zinc in the subarctic North Pacific and Bering Sea: Its distribution, speciation, and importance to primary producers, Global Biogeochem. Cy., 26, GB2015, doi:10.1029/2010gb004004, 2012.

Kellogg, M.M., McIlvin, M.R., Vedamati, J.,Twining, B.S., Moffett, J.W., Marchetti, A., Moran, D.M., and Saito, M.A.: Efficient zinc/cobalt inter-replacement in northeast Pacific diatoms and relationship to high surface dissolved Co:Zn ratios, Limnol. Oceanogr., 9999, 1-26, doi:10.1002/lno.11471, 2020.

Lane, T. W., and Morel, F. M. M.: Regulation of carbonic anhydrase expression by zinc, cobalt, and carbon dioxide in the marine diatom Thalassiosira weissflogii, Plant Physiol., 123, 345-352, doi:10.1104/Pp.123.1.345, 2000.

Largier, J. L., Chapman, P., Peterson, W. T., and Swart, V. P.: The western Agulhas Bank: circulation, stratification and ecology, S Afr J Marine Sci, 12, 319-339, doi:10.2989/02577619209504709, 1992.

Leblanc, K., Hare, C. E., Boyd, P. W., Bruland, K. W., Sohst, B., Pickmere, S., Lohan, M. C., Buck, K., Ellwood, M., and Hutchins, D. A.: Fe and Zn effects on the Si cycle and diatom community structure in two contrasting high and low-silicate HNLC areas, Deep-Sea Res. Pt I, 52, 1842-1864, doi:10.1016/j.dsr.2005.06.005, 2005.

Lee, J. G., and Morel, F. M. M.: Replacement of zinc by cadmium in marine phytoplankton, Mar. Ecol. Prog. Ser., 127, 305-309, doi:10.3354/Meps127305, 1995.

Little, S. H., Vance, D., McManus, J., and Severmann, S.: Key role of continental margin sediments in the oceanic mass balance of Zn and Zn isotopes, Geology, 44, 207-210, doi:10.1130/G37493.1, 2016.

Lutjeharms, J. R. E.: Three decades of research on the greater Agulhas Current, Ocean Sci., 3, 129-147, doi:10.5194/os-3-129-2007, 2007.

Lutjeharms, J. R. E., and Cooper, J.: Interbasin leakage through Agulhas current filaments, Deep-Sea Res. Pt I, 43, 213-238, doi:10.1016/0967-0637(96)00002-7, 1996.

Mackey, M. D., Mackey, D. J., Higgins, H. W., and Wright, S. W.: Chemtax - a program for estimating class abundances from chemical markers: Application to HPLC measurements of phytoplankton, Mar. Ecol. Prog. Ser., 144, 265-283, doi:10.3354/meps144265, 1996.

Mahaffey, C., Reynolds, S., Davis, C. E., and Lohan, M. C.: Alkaline phosphatase activity in the subtropical ocean: Insights from nutrient, dust and trace metal addition experiments, Front. Mar. Sci., 1, doi:10.3389/fmars.2014.00073, 2014.

Martiny, A. C., Lomas, M. W., Fu, W., Boyd, P. W., Chen, Y. L., Cutter, G. A., Ellwood, M. J., Furuya, K., Hashihama, F., Kanda, J., Karl, D. M., Kodama, T., Li, Q. P., Ma, J., Moutin, T., Woodward, E. M. S., and Moore, J. K.: Biogeochemical controls of surface ocean phosphate, Sci. Adv., 5, eaax0341, doi:10.1126/sciadv.aax0341, 2019.

McLennan, S. M.: Relationships between the trace element composition of sedimentary rocks and upper continental crust, Geochem. Geophy. Geosy., 2, doi:10.1029/2000gc000109, 2001.

Menzel Barraqueta, J. L., Klar, J. K., Gledhill, M., Schlosser, C., Shelley, R., Planquette, H. F., Wenzel, B., Sarthou, G., and Achterberg, E. P.: Atmospheric deposition fluxes over the Atlantic Ocean: A GEOTRACES case study, Biogeosciences, 16, 1525-1542, doi:10.5194/bg-16-1525-2019, 2019.

Middag, R., de Barr, H.J.W., and Bruland, K.W.: The relationships between dissolved zinc and major nutrients phosphate and silicate along the GEOTRACES GA02 transect in the western Atlantic Ocean, Global Biogeochem. Cy., 33, 63-84, doi.org/10.1029/2018GB006034, 2019.

Milne, A. C., Schlosser, C., Wake, B. D., Achterberg, E. P., Chance, R., Baker, A. R., Forryan, A., and Lohan, M. C.: Particulate phases are key in controlling dissolved iron concentrations in the (sub)tropical North Atlantic, Geophys. Res. Lett., 44, 2377-2387, doi:10.1002/2016GL072314, 2017.

Moore, C. M.: Diagnosing oceanic nutrient deficiency, Philisophical Transactions of the Royal Society A: Mathmatical, Physical and Engineering Sciences, 374, doi:10.1098/rsta.2015.0290, 2016.

Moore, C. M., Mills, M. M., Arrigo, K. R., Berman-Frank, I., Bopp, L., Boyd, P. W., Galbraith, E. D., Geider, R. J., Guieu, C., Jaccard, S. L., Jickells, T. D., La Roche, J., Lenton, T. M., Mahowald, N. M., Marañón, E., Marinov, I., Moore, J. K., Nakatsuka, T., Oschlies, A., Saito, M. A., Thingstad, T. F., Tsuda, A., and Ulloa, O.: Processes and patterns of oceanic nutrient limitation, Nat. Geosci., 6, 701-710, doi:10.1038/ngeo1765, 2013.

Moore, J. K., and Abbott, M. R.: Phytoplankton chlorophyll distributions and primary production in the Southern Ocean, J. Geophys. Res-Oceans, 105, 28709-28722, doi:10.1029/1999jc000043, 2000.

Morel, F. M. M.: The co-evolution of phytoplankton and trace element cycles in the oceans, Geobiology, 6, 318-324, doi:10.1111/j.1472-4669.2008.00144.x, 2008.

Morel, F. M. M., Reinfelder, J. R., Roberts, S. B., Chamberlain, C. P., Lee, J. G., and Yee, D.: Zinc and carbon co-limitation of marine-phytoplankton, Nature, 369, 740-742, doi:10.1038/369740a0, 1994.

Noble, A. E., Ohnemus, D. C., Hawco, N. J., Lam, P. J., and Saito, M. A.: Coastal sources, sinks and strong organic complexation of dissolved cobalt within the US North Atlantic GEOTRACES transect GA03, Biogeosciences, 14, 2715–2739, doi:10.5194/bg-14-2715-2017, 2017.

Ohnemus, D. C., and Lam, P. J.: Cycling of lithogenic marine particles in the US GEOTRACES North Atlantic transect, Deep-Sea Res. Pt II, 116, 283-302, doi:10.1016/j.dsr2.2014.11.019, 2015.

Ohnemus, D. C., Auro, M. E., Sherrell, R. M., Lagerstrom, M., Morton, P. L., Twining, B. S., Rauschenberg, S., and Lam, P. J.: Laboratory intercomparison of marine particle digestions including Piranha: A novel chemical method for dissolution of polyethersulfone filters, Limnol. Oceanogr-Meth., 12, 530-547, doi:10.4319/lom.2014.12.530, 2014.

Palter, J. B., Sarmiento, J. L., Gnanadesikan, A., Simeon, J., and Slater, R. D.: Fueling export production: nutrient return pathways from the deep ocean and their dependence on the Meridional Overturning Circulation, Biogeosciences, 7, 3549-3568, doi:10.5194/bg-7-3549-2010, 2010.

Paul, M., van de Flierdt, T., Rehkämper, M., Khondoker, R., Weiss, D., Lohan, M. C., and Homoky, W. B.: Tracing the Agulhas leakage with lead isotopes, Geophys. Res. Lett., 42, 8515-8521, doi:10.1002/2015gl065625, 2015.

Price, N. M., and Morel, F. M. M.: Cadmium and cobalt substitution for zinc in a marine diatom, Nature, 344, 658-660, doi:10.1038/344658a0, 1990.

Raux, E., Schubert, H. L., and Warren*, M. J.: Biosynthesis of cobalamin (vitamin B12): A bacterial conundrum, Cell. Mol. Life Sci., 57, 1880-1893, doi:10.1007/PL00000670, 2000.

Rodionov, D. A., Vitreschak, A. G., Mironov, A. A., and Gelfand, M. S.: Comparative genomics of the vitamin B12 metabolism and regulation in prokaryotes, J. Biol. Chem., 278, 41148-41159, doi:10.1074/jbc.M305837200, 2003.

Saito, M. A., and Goepfert, T. J.: Zinc-cobalt colimitation of Phaeocystis antarctica, Limnol. Oceanogr., 53, 266-275, doi:10.4319/lo.2008.53.1.0266, 2008.

Saito, M. A., and Moffett, J. W.: Temporal and spatial variability of cobalt in the Atlantic Ocean, Geochim. Cosmochim. Ac., 66, 1943-1953, doi:10.1016/S0016-7037(02)00829-3, 2002.

740 Saito, M. A., Rocap, G., and Moffett, J. W.: Production of cobalt binding ligands in a
741 Synechococcus feature at the Costa Rica upwelling dome, Limnol. Oceanogr., 50, 279-290,
742 doi:10.4319/lo.2005.50.1.0279, 2005.

743 Saito, M. A., Moffett, J. W., Chisholm, S. W., and Waterbury, J. B.: Cobalt limitation and
744 uptake in Prochlorococcus, Limnol. Oceanogr., 47, 1629-1636,
745 doi:10.4319/lo.2002.47.6.1629, 2002.

746 Saito, M. A., Goepfert, T. J., Noble, A. E., Bertrand, E. M., Sedwick, P. N., and DiTullio, G.
747 R.: A seasonal study of dissolved cobalt in the Ross Sea, Antarctica: Micronutrient behavior,
748 absence of scavenging, and relationships with Zn, Cd, and P, Biogeosciences, 7, 4059-4082,
749 doi:10.5194/bg-7-4059-2010, 2010.

750 Saito, M. A., Noble, A. E., Hawco, N., Twining, B. S., Ohnemus, D. C., John, S. G., Lam, P.,
751 Conway, T. M., Johnson, R., Moran, D., and McIlvin, M.: The acceleration of dissolved
752 cobalt's ecological stoichiometry due to biological uptake, remineralization, and scavenging in
753 the Atlantic Ocean, Biogeosciences, 14, 4637-4662, doi:10.5194/bg-14-4637-2017, 2017.

754 Sarmiento, J. L., Gruber, N., Brzezinski, M. A., and Dunne, J. P.: High-latitude controls of
755 thermocline nutrients and low latitude biological productivity, Nature, 427, 56-60,
756 doi:10.1038/Nature02127, 2004.

757 Schlitzer, R., Anderson, R. F., Dodas, E. M., Lohan, M., Geibert, W., Tagliabue, A., et al.: The
758 GEOTRACES intermediate data product 2017, Chemical Geology, 493, 210-223, 2018.

759 Shaked, Y., Xu, Y., Leblanc, K., and Morel, F. M. M.: Zinc availability and alkaline
760 phosphatase activity in Emiliania huxleyi: Implications for Zn-P co-limitation in the ocean,
761 Limnol. Oceanogr., 51, 299-309, doi:10.4319/lo.2006.51.1.0299, 2006.

762 Sunda, W. G., and Huntsman, S. A.: Feedback interactions between zinc and phytoplankton in
763 seawater, Limnol. Oceanogr., 37, 25-40, doi:10.4319/lo.1992.37.1.0025 1992.

764 Sunda, W. G., and Huntsman, S. A.: Cobalt and zinc interreplacement in marine phytoplankton:
765 biological and geochemical implications, Limnol. Oceanogr., 40, 1404-1417,
766 doi:10.4319/lo.1995.40.8.1404, 1995.

767 Sunda, W. G., and Huntsman, S. A.: Control of Cd concentrations in a coastal diatom by
768 interactions among free ionic Cd, Zn, and Mn in seawater, Environ. Sci. Technol., 32, 2961-
769 2968, doi:10.1021/es980271y, 1998.

770 Sunda, W. G., and Huntsman, S. A.: Effect of Zn, Mn, and Fe on Cd accumulation in
771 phytoplankton: Implications for oceanic Cd cycling, Limnol. Oceanogr., 45, 1501-1516,
772 doi:10.4319/lo.2000.45.7.1501, 2000.

773 Tagliabue, A., Hawco, N. J., Bundy, R. M., Landing, W. M., Milne, A., Morton, P. L., and
774 Saito, M. A.: The role of external inputs and internal cycling in shaping the global ocean cobalt
775 distribution: insights from the first cobalt biogeochemical model, Global Biogeochem. Cy., 32,
776 594-616, doi:10.1002/2017gb005830, 2018.

777 Twining, B. S., and Baines, S. B.: The trace metal composition of marine phytoplankton, Annu.
778 Rev. Mar. Sci., 5, 191-215, doi:10.1146/annurev-marine-121211-172322, 2013.

779 Vance, D., Little, S. H., de Souza, G. F., Khatiwala, S., Lohan, M. C., and Middag, R.: Silicon
780 and zinc biogeochemical cycles coupled through the Southern Ocean, Nat. Geosci., 10, 202-
781 206, doi:10.1038/ngeo2890, 2017.

782 Weber, T., John, S., Tagliabue, A., and DeVries, T.: Biological uptake and reversible
783 scavenging of zinc in the global ocean, Science, 361, 72-76, doi:10.1126/science.aap8532,
784 2018.

785 Woodward, E. M. S., and Rees, A. P.: Nutrient distributions in an anticyclonic eddy in the
786 northeast Atlantic Ocean, with reference to nanomolar ammonium concentrations, Deep-Sea
787 Res. Pt II, 48, 775-793, doi:10.1016/S0967-0645(00)00097-7, 2001.

788 Wu, J. F., Sunda, W., Boyle, E. A., and Karl, D. M.: Phosphate depletion in the western North
789 Atlantic Ocean, Science, 289, 759-762, doi:10.1126/science.289.5480.759, 2000.

790 Wyatt, N. J., Milne, A., Woodward, E. M. S., Rees, A. P., Browning, T. J., Bouman, H. A.,
791 Worsfold, P. J., and Lohan, M. C.: Biogeochemical cycling of dissolved zinc along the
792 GEOTRACES South Atlantic transect GA10 at 40°S, Global Biogeochem. Cy., 28, 44-56,
793 doi:10.1002/2013gb004637, 2014.

794 Xu, Y., Tang, D., Shaked, Y., and Morel, F. M. M.: Zinc, cadmium, and cobalt
795 interreplacement and relative use efficiencies in the coccolithophore Emiliania huxleyi,
796 Limnol. Oceanogr., 52, 2294-2305, doi:10.4319/lo.2007.52.5.2294, 2007.

797 Zubkov, M. V., Fuchs, B. M., Tarran, G. A., Burkill, P. H., and Amann, R.: High rate of uptake
798 of organic nitrogen compounds by Prochlorococcus cyanobacteria as a key to their dominance
799 in oligotrophic oceanic waters, Appl. Environ. Microb., 69, 1299–1304,
800 doi:10.1128/aem.69.2.1299-1304.2003, 2003.

801

802

803

804 Table 1. Analytical validation results for open ocean surface seawater (SAFe S), 1000 m
805 seawater (SAFe D2) and 2000 m seawater (GEOTRACES GD). All concentrations are in nM
806 ($\pm$ 1 std. dev.). Consensus value conversion = 1.025 kg/L. ND indicates sample not determined.

807

	SAFe S	SAFe D2	GEOTRACES GD
Zn (FIA)	0.060 (0.020) $n = 7$	7.723 (0.091) $n = 12$	ND
Zn consensus value	0.071 (0.010)	7.616 (0.256)	1.753 (0.123)
Co (FIA)	0.004 (0.001) $n = 3$	0.049 (0.001) $n = 2$	0.073 (0.004) $n = 5$
Co consensus value	0.005 (0.001)	0.047 (0.003)	0.067 (0.001)

808

809

810 Table 2. Southeast Atlantic dissolved micro- and macronutrient mean concentration inventories
811 for the upper water column during early spring (D357-1), late spring (D357-2) and summer

 (JC068) transects. STSW and SASW waters were defined using the θ 15°C isotherm (Section
813 3.4) and are compared with total inventories calculated for the shallower mixed layer (in
814 parenthesis) that include continental inputs of dissolved Zn and Co. Zn/PO_4^{3-}, Co/PO_4^{3-} and
815 Zn/Co represent the concentration inventory ratios for STSW and SASW, respectively. STSW
816 = Sub-Tropical Surface Water, SASW = Sub-Antarctic Surface Water.

817

818

Oceanographic Regime	Transect	Zn (nmol m⁻³)	Co	NO₃⁻	PO₄³⁻ (µmol m⁻³)	Si(OH)₄	Zn/PO₄³⁻ (µmol mol⁻¹)	Co/PO₄³⁻	Zn/Co (mol mol⁻¹)
STSW	Early spring	624 (1597)	32 (30)	2694 (870)	333 (203)	3735 (2790)	1876	97	19
	Late spring	384 (592)	23 (17)	1846 (763)	276 (191)	2781 (2326)	1387	82	17
	Summer	158 (139)	29 (24)	1557 (326)	226 (139)	2711 (1942)	699	129	5
SASW	Early spring	182 (112)	14 (13)	6035 (5300)	615 (566)	1875 (1847)	296	22	13
	Summer	83 (94)	12 (10)	4143 (3388)	439 (400)	1027 (886)	188	26	7

819

820

821

822

823
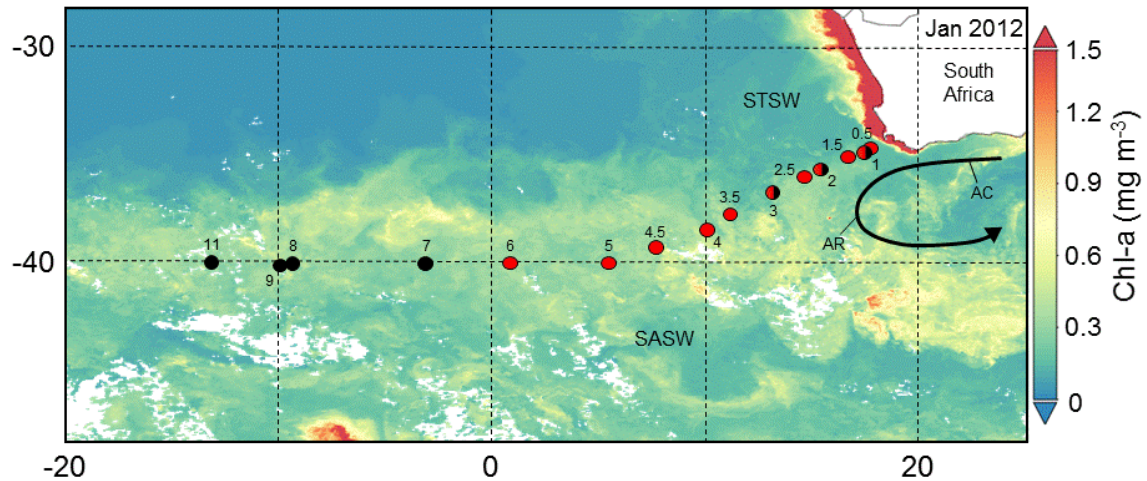
824 Figure 1. The Southeast Atlantic stations sampled for dissolved Zn and Co along the GA10
825 section during UK-GEOTRACES cruises D357 (red circles) and JC068 (black circles),
826 overlain a VIIRS monthly composite image of chlorophyll-*a* concentrations for January 2012
827 (https://oceancolor.gsfc.nasa.gov/). Two transects were completed during D357 between Cape
828 Town and the zero meridian that represent early austral spring 2010 (D357-1; Stns. 1, 2, 3, 4,
829 5 & 6) and late austral spring 2010 (D357-2; Stns. 0.5, 1, 1.5, 2.5, 3.5, 4.5), respectively. JC068
830 took place during austral summer 2011/12 and we present here only the repeat transect data

between Cape Town and 13°W (Stns. 1, 2, 3, 7, 8, 9, 11). STSW = Sub-Tropical Surface Water, SASW = Sub-Antarctic Surface Water, AC = Agulhas Current, AR = Agulhas retroflection.

833

834
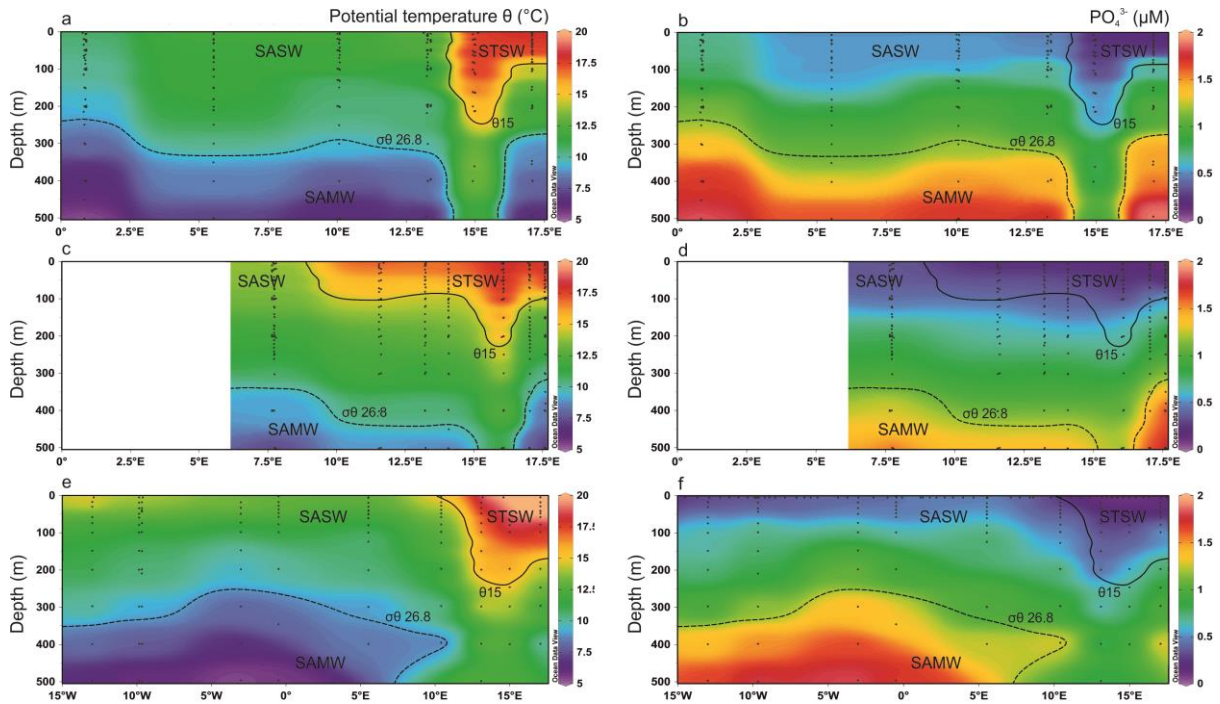
Figure 2. Upper 500 m potential temperature (θ) and dissolved PO_4^{3-} distributions for the Southeast Atlantic along early spring (a,b; D357-1), late spring (c,d; D357-2) and summer (e,f; JC068) transects. The dominant Southern Ocean (SASW & SAMW) and South Atlantic (STSW) water masses that influence the distribution of nutrients are shown. The θ 15°C isotherm (solid contour) represents a practical definition of the STF location, whilst SAMW is identified by the median potential density (σθ) isopycnal 26.8 kg m^{-3} (dashed contour, see Sect. 4.1.). STSW = Sub-Tropical Surface Water, SAMW = Sub-Antarctic Mode Water, AAIW = Antarctic Intermediate Water.

843

844

845
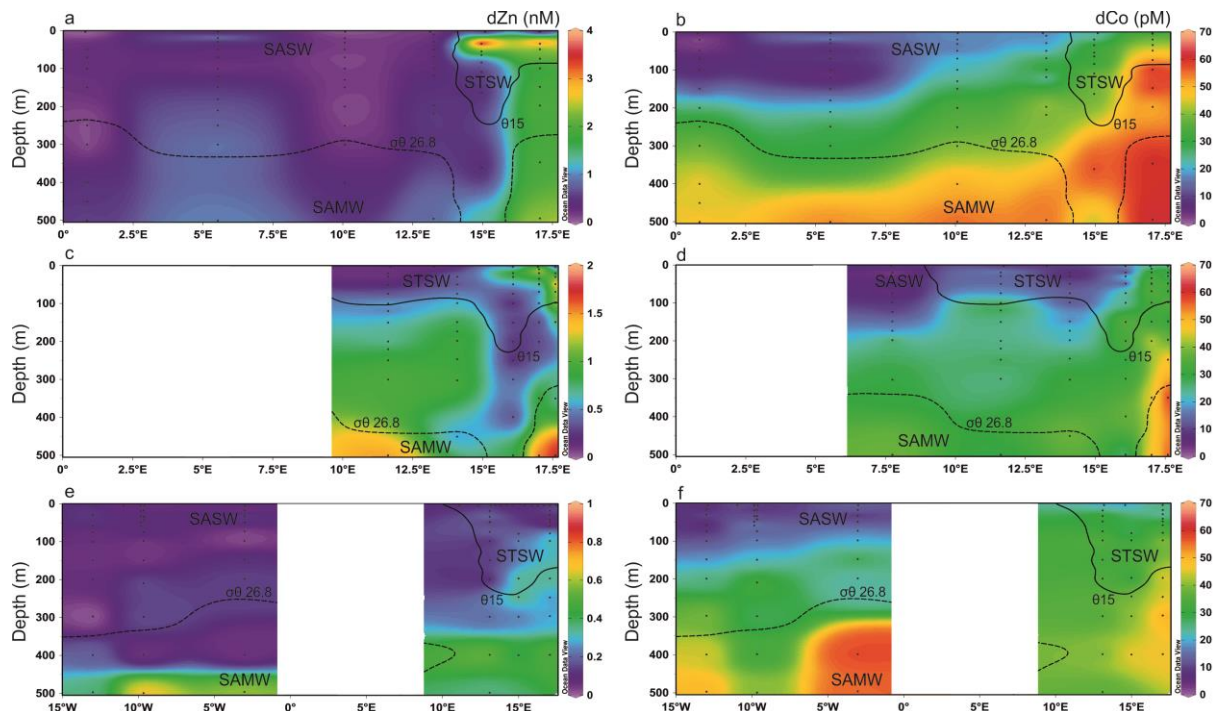
846 Figure 3. Upper 500 m dissolved Zn and Co distributions for the Southeast Atlantic along early
847 spring (a,b; D357-1), late spring (c,d; D357-2) and summer (e,f; JC068) transects. The STF is
848 delineated by θ 15°C (solid contour), whilst the influence of SAMW is evident by the median
849 potential density (σθ) isopycnal 26.8 kg m^{-3} (dashed contour, see Section 4.1.). STSW = Sub-
850 Tropical Surface Water, SAMW = Sub-Antarctic Mode Water, AAIW = Antarctic Intermediate
851 Water. Note the changing y-axis scales for dZn distribution.

852

853
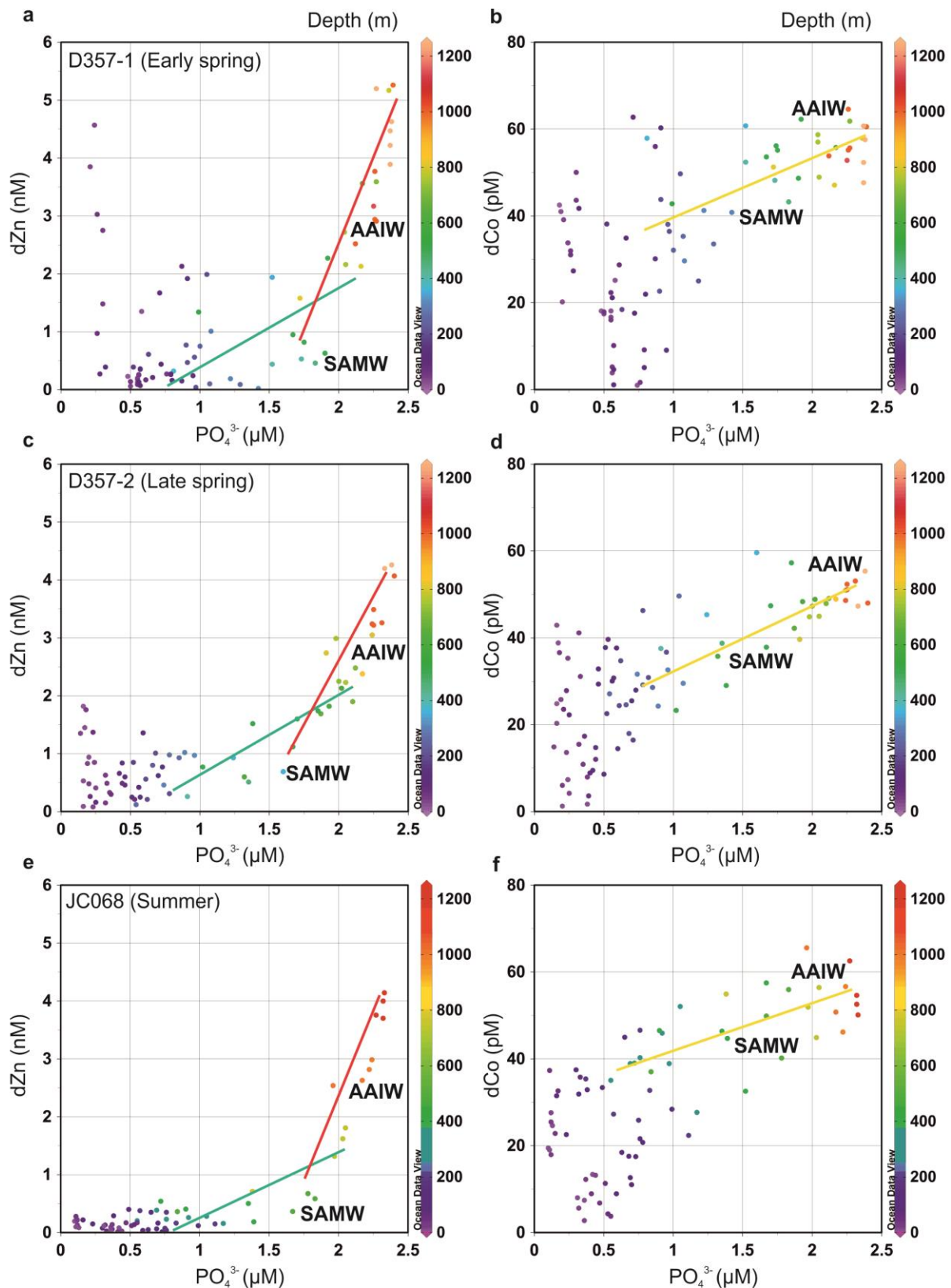
Figure 4. The dissolved Zn and Co versus PO_4^{3-} distribution for the Southeast Atlantic during early spring (a,b; D357-1), late spring (c,d; D357-2) and summer (e,f; JCO68) transects. The green and red lines indicate the $dZn:PO_4^{3-}$ regression slopes for SAMW and AAIW, respectively. The yellow line indicates the $dCo:PO_4^{3-}$ regression slope for SAMW and AAIW combined. The equations for regression lines are detailed in Supplementary table 1. SAMW =

859 Sub-Antarctic Mode Water, AAIW = Antarctic Intermediate Water. The full depth dZn:PO$_4^{3-}$
860 relationship along JC068 can be found in Wyatt et al. (2014).

861

862

863
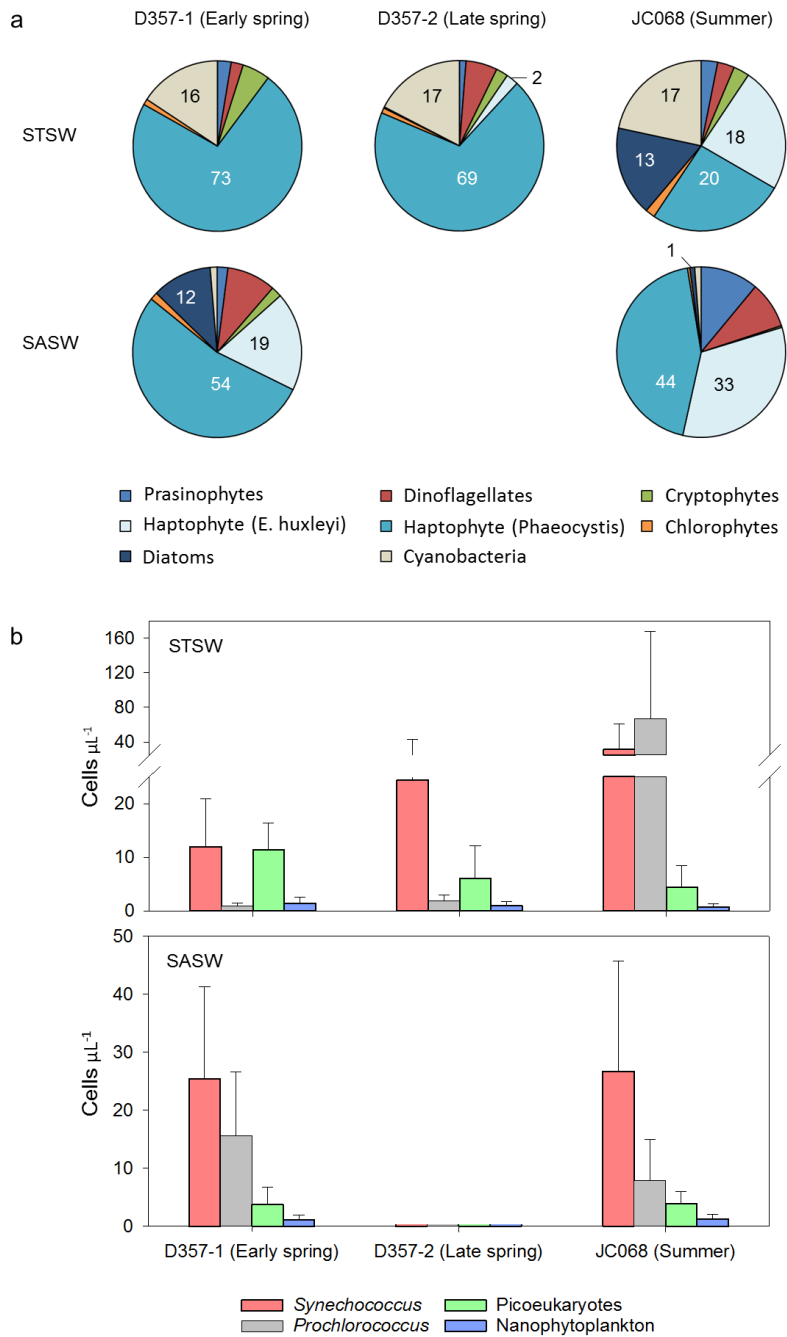
864 Figure 5. Seasonal differences in (a) pigment-derived taxonomic contributions to total
865 chlorophyll-*a* (percentage), and (b) AFC counts of *Synechococcus, Prochlorococcus,*
866 nanophytoplankton (approx. >2µm) and photosynthetic picoeukaryotes (approx. <2µm) in the
867 Southeast Atlantic.

868

869
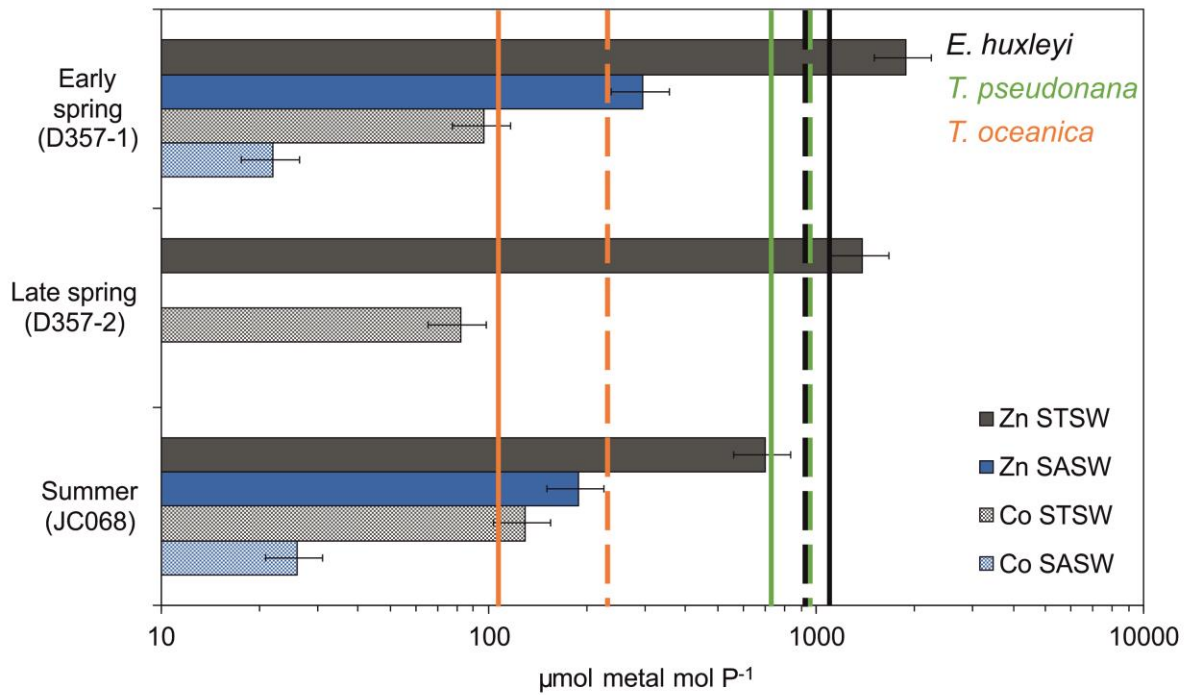
870 Figure 6. Metal/PO$_4$$^{3-}$ inventory ratios for the upper water column of the Southeast Atlantic
871 (horizontal bars) compared with laboratory estimates of cellular ratios in eukaryotic
872 phytoplankton below which growth limitation occurs (solid vertical lines represent Zn:P with
873 no added Co to media whilst dashed lines represent Co:P with no added Zn; phytoplankton
874 data from Sunda and Hunstman, 1995). Error bars on inventory ratios represent 20 % combined
875 uncertainty for dZn and dCo analyses (see Section 2.2). This figure is adapted from that in Saito
876 et al. (2010) and implies that inter-seasonal differences in metal/PO$_4$$^{3-}$ stoichiometry could
877 impact phytoplankton community composition in the Southeast Atlantic.

878

879

880